UFSM

CIÊNCIA e NATURA

ISSN 2179-460X
Acesso aberto

Ci. e Nat., Santa Maria, v. 44, e46, 2022 • https://doi.org/10.5902/2179460X65529
Submitted: 30/04/2021 • Approved: 18/10/2021 • Published: 24/11/2022

Meteorology

Characteristics of a hailstorm that occurred in Santa Rita do Sapucaí-MG, Brazil, in October 2019

Características do evento convectivo ocorrido em Santa Rita do Sapucaí-MG em outubro de 2019

Bruna Andrelina [I], Michelle Simões Reboita [I], Bruno César Capucin [I], Enrique Vieira Mattos [I], Larissa Helena da da Costa [I], Diego Pereira Enoré [II], Thiago Souza Biscaro [III]

[I] Universidade Federal de Itajubá, Itajubá, MG, Brazil
[II] Instituto Nacional de Pesquisas Espaciais, São José dos Campos, SP, Brazil
[III] Instituto Nacional de Pesquisas Espaciais, Cachoeira Paulista, SP, Brazil

ABSTRACT

Santa Rita do Sapucaí is a city located in south Minas Gerais (MG) state, Brazil. On October 24th, 2019, at 20:00 UTC, a hailstorm struck the city, causing widespread damage. This study evaluates the meteorological conditions that led to the storm formation using a multiscale approach i.e., analyzing the synoptic, mesoscale, and physical properties of the thunderstorm using collected data from different sources. The synoptic analysis showed that the thunderstorm developed in response to the dynamic (wind divergence at upper levels that causes upward movements) and thermodynamic (instability) processes in the atmosphere. This was a Severe Storm (SS), according to the Potential for Severity and Hail index. The relationship between CAPE and vertical wind shear, in conjunction with radar images, showed that the thunderstorm started as a multicellular system. The thunderstorm was characterized by deep clouds tops, intense ice production, and high intra-cloud (up to 160 min^{-1}) and cloud-to-ground (up to 20 min^{-1}) lightning rates before the hail precipitated, showing that these lightning data can be used to predict surface hail precipitation.

Keywords: Convective thunderstorm; Hail; Soft hail; Lightning

RESUMO

A cidade de Santa Rita do Sapucaí, localizada no sul do Estado de Minas Gerais (MG), no dia 24 de outubro de 2019 a cerca de 2000 UTC foi atingida por uma tempestade de granizo que gerou diversos danos ao município. O presente estudo avalia as condições meteorológicas que propiciaram a ocorrência da tempestade com enfoque multiescala (sinótica, mesoescala e microfísica da tempestade). A análise

sinótica mostrou que a tempestade se desenvolveu como uma resposta da dinâmica (divergência do vento em altos níveis que propiciou os movimentos ascendentes na coluna atmosférica) e termodinâmica (instabilidade) da atmosfera. A relação entre CAPE e cisalhamento vertical do vento, bem como imagens de radar, indicam que a tempestade foi multicelular. A tempestade foi caracterizada por topos profundos, intensa produção de gelo e alta taxa de relâmpagos intra-nuvem (até 160 por min) e nuvem-solo (até 20 por min) antes da ocorrência do granizo, indicando o potencial do uso de dados de relâmpagos como um parâmetro preditor da ocorrência de granizo em superfície.

Palavras-chave: Santa Rita do Sapucaí; Tempestade convectiva; Granizo; Relâmpagos

1 INTRODUCTION

Santa Rita do Sapucaí (SRS) city is located in south Minas Gerais (MG) state in Brazil (Figure 1). The area is geographically characterized by alternating mountains and valleys that form the Sapucaí river basin. According to a 2010 census, the population of SRS was approximately 37,700 inhabitants (IBGE, 2020). SRS is also called the “Silicon Valley of Brazil”, since it is a very important national and internationally recognized region of technological development in Brazil (INATEL, 2020).

In the late afternoon of October 24th, 2019, SRS was struck by a thunderstorm that produced hail, which lasted for approximately 30 minutes (Figure 1) (Journal G1, 2019). That day, the Civil Defense Department had issued several alerts for intense precipitation in south MG, including hail warnings between 17:00 and 19:00 local time (20:00-22:00 UTC), the same moment that the thunderstorm reached SRS city (ESTADO DE MINAS, 2019). The hailstorm caused structural damage at a gas station, damaged industrial warehouses, shattered the windows of some vehicles, collapsed school roofs, and led to the death of one resident who tried to take shelter under a tree that fell, in addition to destroying the roofs of many houses and knocking down many trees (Figure 1 - Jornal G1, 2019). According to the energy concessionaire in SRS, the rain also caused damage to electrical systems, interrupting energy supplies in several parts of the city (UOL Notícias, 2019).

According to Wallace and Hobbs (2006) and Alcântara (2011), the formation of a typical storm is associated with a combination of some factors as: (1) air-lifting

mechanisms, such as wind combined with a topographic barrier (dynamic factor) or convection (thermodynamic factor); (2) humid rising air; (3) instability, as moving air must be warmer than the layers where it travels; and (4) vertical wind shear in the layer between the surface and 6 km, which can neither be too weak nor too intense since clouds cannot form under such circumstances.

Storms can receive the status of severe depending on their physical features and associated damages to society. Studies on the United States found that Severe Storms (SS) were associated with hail, intense downdrafts, and in some cases, tornadoes. According to different studies (Johns and Doswell, 1992; Moller, 2001; Nascimento, 2005), SS can be defined as having at least one of the following characteristics: (1) hail larger than 2 cm and/or (b) destructive wind speeds above 93 km h^{-1} with amplified vortices towards the surface, generating tornadoes. Although this definition was originally created for mid-latitudes in the Northern Hemisphere, it can also be applied to the Southern Hemisphere. Furthermore, heavy rains and flash floods can be included in the SS definition, as was indicated in a SS study from Australia (Mills and Colquhoun, 1998). However, it is harder to establish thresholds for these two latter characteristics, since they depend on regional vulnerabilities in general, and are not applied to SS studies (they are not considered here in our study either).

In Brazil, most SS occur in the south and southeast (Silva Dias and Grammelsbacher, 1991; Martins *et al*., 2017; Beal *et al*., 2020), which are regions mainly influenced by the moisture transported by the Low-Level Jet (LLJ) east of the Andes (Pinheiro *et al*., 2014; Santos and Reboita, 2018; Montini *et al*., 2019). Between mid-spring and mid-autumn, which is the wet period of the South American Monsoon (Reboita *et al*., 2010; Ashfaq *et al*., 2020), the LLJ frequently flows from the Amazon to southeast Brazil, carrying warm and moist air that combine with local convection processes, typical of that period of the year, promoting storm formation. Several precipitation events in southern Minas Gerais (MG) are also associated with moisture supplied from the LLJ and moisture

transport from the Atlantic Ocean via winds from the South Atlantic Subtropical Anticyclone (Reboita *et al*., 2010; Silva *et al*., 2019; Marengo *et al*., 2020). For example, major floods in southern MG in 1991 and 2000 occurred in the summer, when these systems were present, leading to South Atlantic Convergence Zone (SACZ) episodes (Reboita *et al*., 2017). Additionally, rainfall in SRS may also be influenced by the circulation of mountain valley breezes (mesoscale phenomenon).

In terms of hail climatology in South America, many hail storms occur in northern Argentina, extending to Paraguay, Uruguay, and parts of Brazil and Bolivia (Cecil and Blankenship, 2012; Beal *et al*., 2020). In Brazil, most hailstorms occur in southern states, followed by south-southeast MG, Espírito Santo, and Rio de Janeiro (Martins *et al*., 2017). Hailstorms are seasonally variable, with more storms in spring and summer (Barnes, 2001, Martins *et al*. 2017; Beal *et al*. 2020). This can be explained by strong diurnal surface heating, triggering convective activity, and, consequently, storm formation.

There is not much literature addressing the physical characteristics of severe storms in Brazil i.e., duration, vertical extent, top temperature, type of lightning, etc. However, Kneib (2004), Nascimento (2005), Tavares and Mota (2012), Silva Neto (2014), Abreu *et al*. (2020), and Mattos *et al*. (2020) have conducted such studies. Kneib (2004) described the characteristics of two Squall Lines (SL) that affected Paraná state. On 9 August 1999, a line developed parallel to a surface cold front, with an average duration of 4 h and 30 min and an average speed at 12.9 m s^{-1}. The case study (12/24/2000) also showed perpendicular surface cold fronts. The author also emphasized the importance of monitoring SL, since these systems can cause rapid changes in weather conditions, resulting in windstorms or floods. Abreu *et al*. (2020) evaluated the microphysical and electrical parameters of nine hailstorms that occurred in São Paulo state, and emphasized that the Waldvogel Height (AW), which is a method for estimating hail in storm cells, can predict hail events up to 20 minutes prior to their onset, showing a high probability of hail precipitation in storms. Mattos *et al*. (2020) studied the synoptic, thermodynamic, and physical

aspects of a storm that caused severe weather in Bauru (SP). These authors showed that lightning peaks occurred 23 minutes before hail struck, and stated that this information could be used to predict severe events. Other studies have been dedicated to analyzing the damage caused by storms, e.g., Gatti (2019), who evaluated the impacts of 9 SS associated with Mesoscale Convective System (MSC) formations in Santa Catarina state.

The mentioned studies were also important for understanding atmospheric and thermodynamic processes that led to thunderstorm occurrences and significant weather for each region. However, literature still lacks studies related to Brazil, given that it is a very large country, with peculiar regional geographies that contribute differently to storm formation. The objective of this study was to detail the environmental conditions that led to a storm on October 24th, 2019, in Santa Rita do Sapucaí (SRS) (MG), Brazil. We employed a multiscale approach starting with synoptic analysis, which will describe the environmental characteristics of the storm, and continuing with a mesoscale analysis, which will focus on the thunderstorm's thermodynamic aspects, all in an effort to determine the physical properties of the storm, which include the type of lightning, the storm top temperature, etc. This study is the first study that addresses a hailstorm in SRS. Furthermore, understanding the physical formation and occurrence processes of storms can lead to ways of developing new nowcasting tools that could aid in minimizing societal damage.

2 MATERIAL AND METHODS

2.1 Data

Different data sources were used in this study: (1) reanalysis from the European Center for Medium-Range Weather Forecasts (ERA5; Hersbach *et al*., 2020); (2) São Roque radar dataset belonging to the Department of Air Space

Control (DECEA); (3) data from the Geostationary Operational Environmental Satellite-16 (GOES-16) provided by the Center for Weather Forecasting and Climate Studies (CPTEC), from the National Institute for Space Research (INPE); and (4) lightning records from the Earth Networks Total Lightning Network (ENTLN). Figure 1 shows images of the places affected by the hail storm and the radar's action region.

Figure 1 – Left panel: study region and its topography. The black circle represents the maximum detection distance at 240 km from the São Roque (SP) radar. Right panel: car hit by hail, road covered in hail, damaged gas station, and an example of the size of the hail that hit SRS on October 24th, 2019 (*Portal G1*, 2019)

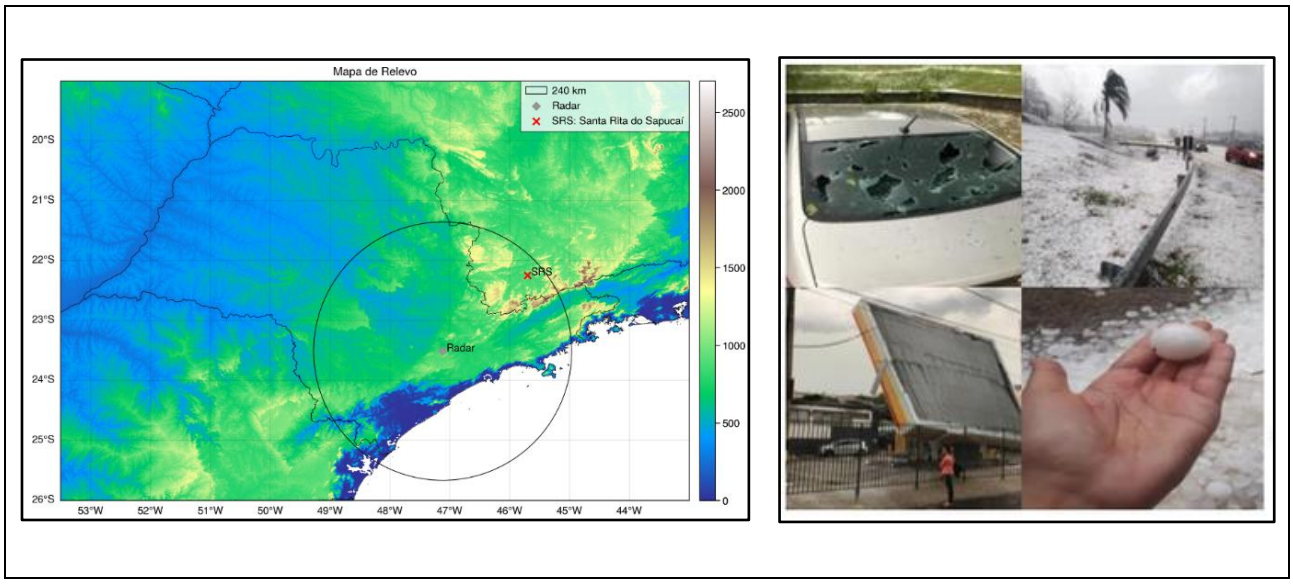

Fonte: Author's (2019)

Although this is a multiscale study, we do not seek to make simulations using mesoscale numerical models. The synoptic scale analysis was performed using ERA5 reanalysis with a 25 km horizontal resolution, allowing us to study phenomena at scales greater than 50 km (2 Δx). Mesoscale characteristics are inferred from satellite and radar data, which were also used to analyze the physical structure of the storm.

2.2 Synoptic and Mesoscale Analysis

ERA5 reanalysis (Hersbach *et al*., 2020) was used to analyze the synoptic environment of the thunderstorm. This reanalysis has a horizontal resolution at approximately 25 km, with an hourly frequency. The variables obtained at the 950, 850, 700, 600, 550, 500, 300, 250, and 200 hPa pressure levels were: geopotential ($m^2\ s^{-2}$), which was later converted to geopotential height (mgp), specific humidity ($g\ kg^{-1}$); vertical velocity ($Pa\ s^{-1}$); mass divergence (s^{-1}); horizontal wind components ($m\ s^{-1}$); air temperature (K); mean sea level pressure (hPa); precipitable water (mm); and Convective Available Potential Energy - CAPE ($J\ kg^{-1}$). Data were obtained for October 22nd to the 24th, 2019. Using these aforementioned variables, we produced the following meteorological fields: (1) mean sea level pressure, and layer thickness 1000/500 hPa, which is the difference between the geopotential height between the 500 and 1000 hPa levels, along with winds at 250 hPa, and mass divergence at 250 hPa (s^{-1}); (2) winds at 250 and 850 hPa, and divergence at 250 hPa, to check if the divergence favored air lifting in the atmospheric column; (3) precipitable water and winds at 850 hPa; and (4) humidity and wind convergence at 850 hPa, along with vertical velocity (omega) at 500 hPa.

Surface synoptic maps from the Center for Weather Forecasting and Climate Studies of National Institute of Space Research (CPTEC/INPE) for the period under study were also obtained to complement the analysis (http://tempo.cptec.inpe.br/). An adapted version of the Potential for Severity and Hail index, which is used worldwide, including South America (WPC, 2020), developed by Gálvez and Santayana (2019), and operationally used by the National Oceanic and Atmospheric Administration (NOAA) Weather Prediction Center (WPC) International Desks (2020) was used here to identify the severity potential of the storm. The storm severity potential index is obtained by combining the following criteria:

(1) temperatures at 500 hPa must be less than -8ºC, making it difficult for the hail to melt as it moves to the surface;

(2) the difference between temperatures at 700 hPa and 500 hPa must be greater than 16ºC ($T_{700} - T_{500} > 16$ ºC), meaning that the 700 hPa layer is warmed, favoring atmospheric instability processes given the presence of warmer layers under colder layers;

(3) vertical velocity in the layers between 600 and 400 hPa must be less than 0 Pa s^{-1}, which indicates upward movements, which is calculated by averaging the omega variable of all vertical levels between 600 and 400 hPa;

(4) the average of specific moisture flux divergence in the layers between 700 hPa and 950 hPa must be less than 0 g kg^{-1} m^{-2}, which indicates convergence;

(5) the average between the vertical wind shear calculated at layers between 6 km (~550 hPa) and 0 km and, 3 km (~700 hPa), and 0 km (~1000 hPa) must be greater than 10 m s^{-1} ($[shear_{6\text{-}0km} + shear_{3\text{-}0km}]/2 > 10$ m s^{-1}), so updrafts and downdrafts inside the clouds will not cancel each other out, so clouds do not dissipate;

(6) divergence between 300 hPa and 200 hPa must be greater than 0 s^{-1}, which induces upward movements in layers closer to the surface, obtained by averaging the divergence between the 300 and 200 hPa levels.

When the six parameters meet the established limits, a region is said to be conducive to SS formation. The difference relative to the original index formulation can be found in criteria (3), (4), (5), and (6). Regarding criterion (3), a more robust omega value is obtained when this variable is analyzed between the non-divergence level (500 hPa) limits. Thus the 600 to 400 hPa levels were used instead of the 600 to 300 hPa levels. Criterion (4) was relaxed relative to the original index formulation, meaning that only less-than-zero moisture flow convergence levels are needed, without imposing index thresholds, e.g., -0.5 x 10^{-8} kg kg^{-1} m^{-2}. Regarding criterion (5), since analysis in some SS cases showed values at 10 m s^{-1}, this threshold was set to a more flexible level than the 20 m s^{-1} level suggested in the original index formulation. Criterion (6) was also relaxed, as a divergence threshold value was not imposed (e.g. 1.3 x 10^{-5} s-1). Positive values are sufficient

for this criterion. These adaptations were made to the index because they are more representative of events that occur in southeastern Brazil.

The SkewT-LogP diagram was prepared, and the CAPE, K, and Total Totals (TT) instability indices were calculated from a mesoscale perspective, to understand the environment in which the storm formed (details on these indices can be found in Ferreira and Reboita, 2020). Since radiosondes are not launched in SRS nor in the surrounding regions, both the diagram and indices were obtained based on ERA5 reanalysis. The Bulk Richardson Number was also calculated (BRN; Moncrieff and Green, 1972; Weisman and Klemp, 1984; Stensrud *et al*., 1997; Thompson *et al*., 2003; NOAA, 2021), which is the ratio between the buoyancy of air parcels (given by CAPE), and vertical wind shear: BRN = CAPE / 0.5 U^2, being U is the difference in wind intensity between 0-6 km i.e., the vertical wind shear. The BRN is a dimensionless quantity, and indicates the balance between buoyancy and vertical wind shear. It is used to distinguish between storm types (Vasquez, 2017), according to the following criteria:

(1) BRN < 10 = weak instability, or very intense vertical shear, or both. This includes storms generated from synoptic forcing and multicellular convective systems;

(2) 10 ≤ BRN ≤ 50 = indicative of supercells; and

(3) BRN > 50 = strong instability, weak vertical shear, or both.

This category includes unit cells and multicellular clusters. By analyzing a set of 413 supercells, Thompson *et al*. (2003) observed that transitions from non-supercell storms to supercell storms, occurred when vertical wind shear increased from 20 to 30 m s^{-1}, while supercells with tornadoes showed vertical wind shears greater than 50 m s^{-1}.

2.3 Physical Characteristics of the Storm

Data from water vapor (WV) and infrared (IR) channels were used to analyze cloud depth. This information came from the Advanced Baseline Imager Sensor (ABI) sensor (Schmit *et al*., 2005) on board the GOES-16 satellite, which has 16 spectral channels, at a temporal resolution of 10 minutes. We employed the methodology proposed by Schmetz *et al*. (1997) to calculate cloud depth, which consists of the difference between the brightness temperature of the WV channel (6.2 μm), and the infrared (10.3 μm) (TWV-TIR) channel. This calculation locates deep clouds capable of penetrating the tropopause and injecting moisture into the lower stratosphere. Positive difference values are associated with overshooting tops, which are characterized by stronger updrafts found in low brightness temperature regions with more lightning activity. Clouds that cross the tropopause can produce high concentrations of ice particles, and are generally indicative of SS (Bedka, 2011).

Precipitation characteristics were analyzed using data from the São Roque radar, São Paulo (SP) state. This radar is operated by the 1st Integrated Center for Air Defense and Air Traffic Control (CINDACTA I), from the Department of Air Space Control (DECEA), located at 23º 36' 07'' S, 47º 05' 39'' W, at 1147 m (Figure 1). This is a Doppler radar operating in the S-band (2.7 GHZ), at a wavelength of 10.89 cm, a pulse width of 1.98 degrees, with a temporal resolution of 10 minutes. Constant Altitude Plan Position Indicator (CAPPI) of reflectivity (dBZ) data with a horizontal and vertical spatial resolution of 1 km, comprising 16 vertical levels from 2 km to 17 km were obtained. The thunderstorms were identified and tracked using the CAPPI 3 km reflectivity data, from its genesis until the moment that the thunderstorm left the radar area. The thunderstorm tracking and spatial delimitation were performed using a polygon centered on the storm that shifted over time (more details in the results section).

The following storm parameters were calculated for each stage of the storm's life cycle: (1) vertically integrated liquid water content (VIL - Greene and Clark, 1972); (2) VIL density (DVIL); (3) Waldvogel height (AW, Waldvogel *et al*., 1979); (4) 20 dBZ top echo; (5) 35 dBZ top echo; (6) maximum column reflectivity; and (7) storm size (area). More details on these parameter calculations can be found in Abreu *et al*. (2020).

The thunderstorm's electrical activity was analyzed using ENTLN data. This network detects strokes using the Earth Network's sensors technology. Currently, the ENTLN covers south, southeast, midwest, and northeast regions of Brazil. ENTLN uses the time-of-arrival (TOA) method to detect emissions from return strokes between 1 Hz and 12 MHz, in real-time. The data were provided by the CLIMATEMPO company. The files were in text format, and contained the following information: date, time, latitude and longitude, and the type of return stroke, i.e., in intra-cloud (IN) or cloud-ground (NS) lightning. The occurrence of return stroke was counted within the polygon over 10-minute intervals for each stage of the storm's life cycle.

3 RESULTS AND DISCUSSION

3.1 Analysis of Synoptic and Mesoscale Characteristics

This section begins with a synoptic description of the two days prior to the day of the thunderstorm, and then focuses on the hours leading up to the storm. Figure 2 shows the synoptic fields between October 22nd and 24th, 2019. No cold fronts were present in southeast Brazil (Figure 2) during this period. On the 22nd of October, an inverted trough appeared in a pressure field at mean sea level (MSLP; Figure 2D), between northern MG, and the Atlantic Ocean, that helped organize the moisture convergence band shown on October 23rd (Figure 2E), but which did not persist past the 24th. In contrast, on the 24th, there was a trough on the surface

between São Paulo (SP) State, and the Atlantic Ocean, that helped configure a low-pressure area. The surface trough and moisture convergence zone regions are characterized by organized band clouds extending from the Amazon towards the Atlantic Ocean (Figure 2A-C).

Figure 2 – Synoptic analysis for October 22nd, 23rd, and 24th, 2019, at 18:00 UTC: (A-C) GOES-16 satellite images of the visible channel (CH2, 0.64 μm), (D-F) surface synoptic charts showing MSLP (hPa, in black), layer thickness 500/1000 hPa (gpm, dashed red lines), and wind magnitude at 250 hPa (m s^{-1}, colored area), and (G-I) mass divergence at 250 hPa (s^{-1}, in green). The box and red circle indicate the study region

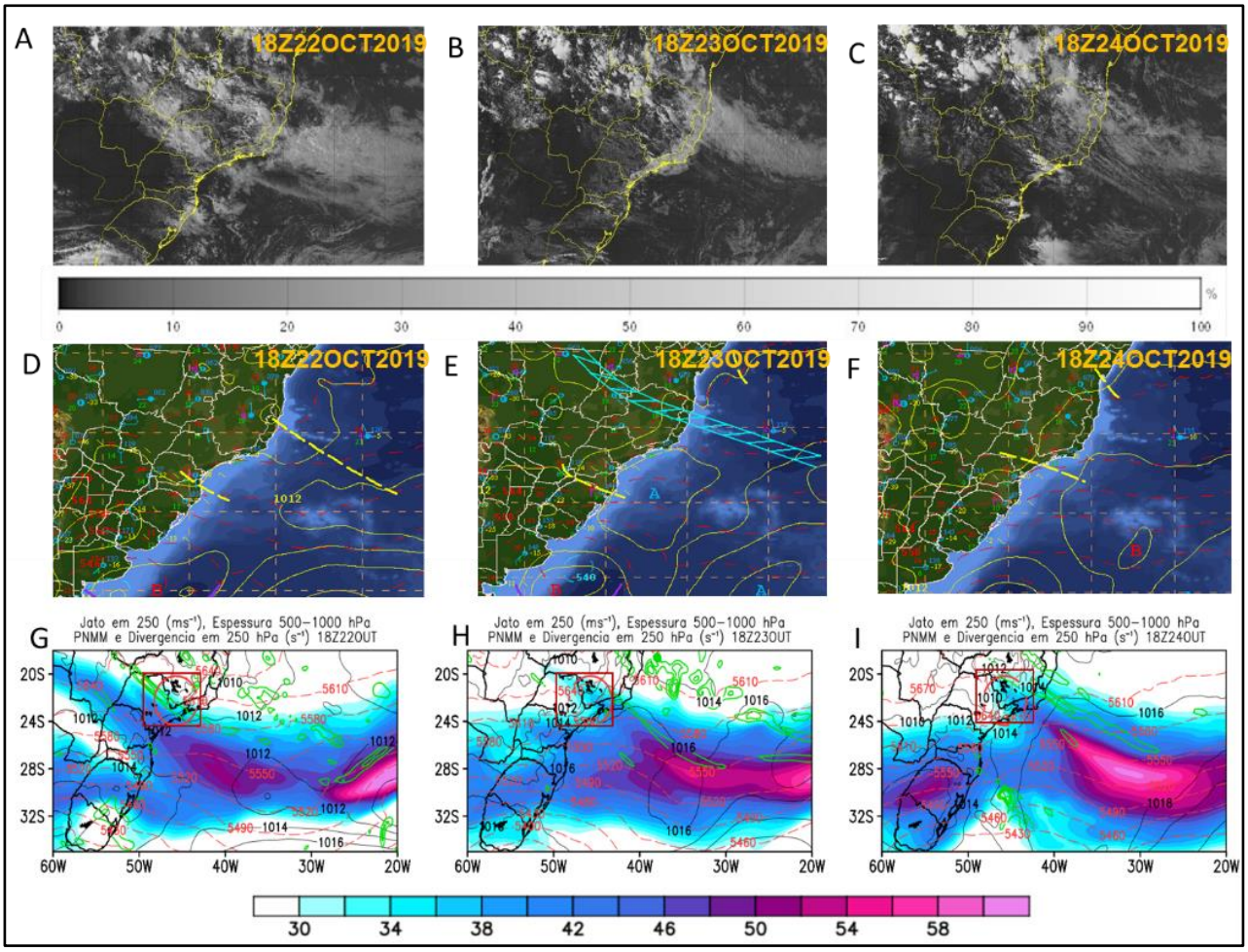

Source: Author's (2019)

Regarding atmospheric circulation at upper levels, from October 22nd to October 24th, 2019, the subtropical jet migrated slightly to the north, so that its northern entrance sector reached Rio de Janeiro (RJ), and south MG (shown in greater detail in Figure 3). There was mass divergence at 250 hPa, as shown by the green lines in Figures 2 G-L, in these sectors.

The synoptic environment before and during the hailstorm in SRS is shown in Figure 3. Figures 3 A-D show the subtropical jet between the continent and the Atlantic Ocean. The jet entrance, i.e., the region where upper-level winds accelerate, was located between SP, MG, and RJ states. Upper wind acceleration led to mass divergence in the upper troposphere (Holton, 2004), which can be identified in yellow color over the southeast. Emphasis should be given to the intensified divergence in the south of MG from 20:00 UTC. In practice, upper-level mass divergence induces upward movements in atmospheric columns, which is important for reducing low-level atmospheric pressure and cloud formation.

The precipitable water and wind at 850 hPa (Figure 3 E-H) showed that moisture was largely advected from the Atlantic Ocean over the southeast via an anticyclonic circulation centered east of the southeast Brazil coastline. However, there were no high precipitable water values in SRS, indicating that not all the tropospheric column was wet. This is also indicated in the SkewT-LogP diagram for SRS (which is shown in Figure 5A), where the troposphere is wetter around 850-800 hPa, and drier at other levels. This moisture profile is important for storm intensification, as will be discussed later. Convergence over south MG (in the SRS region), was observed starting at 20:00 UTC, according to changes in wind directions (from north to south), as per figures 3G-H, in the area extending from east SP to southeast MG, and in the southern flows in the same region, shown in figure 3K-L.

Figure 3 – Synoptic fields at 17:00, 19:00, 20:00, and 21:00 UTC on October 24th, 2019. (A-D) jets at 250 hPa (m s^{-1}; colored), streamlines at 250 hPa (m s^{-1}), and mass divergence at 250 hPa (104 s^{-1}; in yellow), (E-H) precipitable water (mm; colored), wind vectors at 850 hPa (m s^{-1}; in black, with arrows), (I-L) moisture convergence at 850 hPa (106 g $kg^{-1}s^{-1}$; colored), and wind vectors at 850 hPa (m s^{-1})

To be continued...

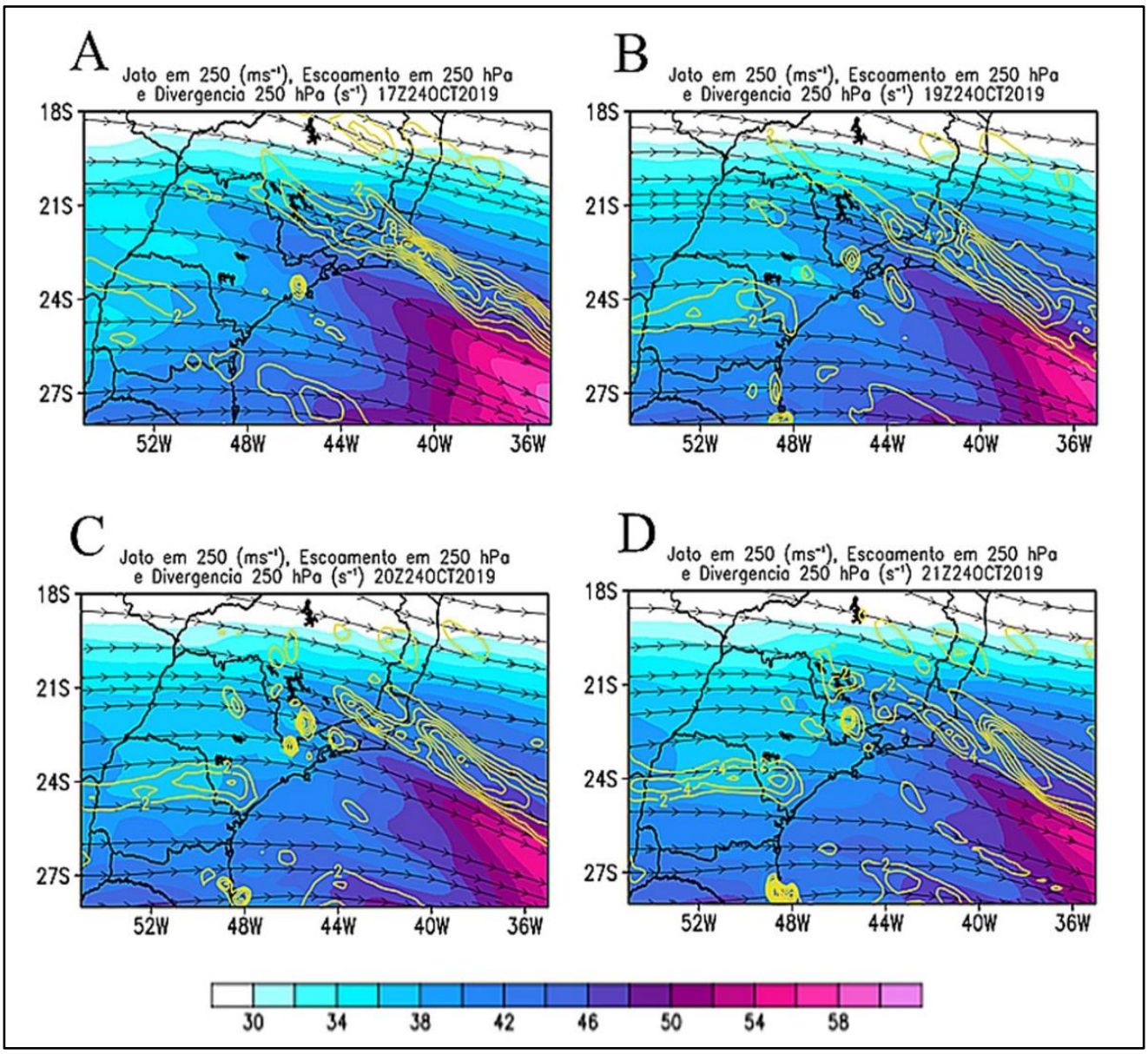

Figure 3 – Synoptic fields at 17:00, 19:00, 20:00, and 21:00 UTC on October 24th, 2019. (A-D) jets at 250 hPa (m s^{-1}; colored), streamlines at 250 hPa (m s^{-1}), and mass divergence at 250 hPa (104 s^{-1}; in yellow), (E-H) precipitable water (mm; colored), wind vectors at 850 hPa (m s^{-1}; in black, with arrows), (I-L) moisture convergence at 850 hPa (106 g $kg^{-1}s^{-1}$; colored), and wind vectors at 850 hPa (m s^{-1})

To be continued...

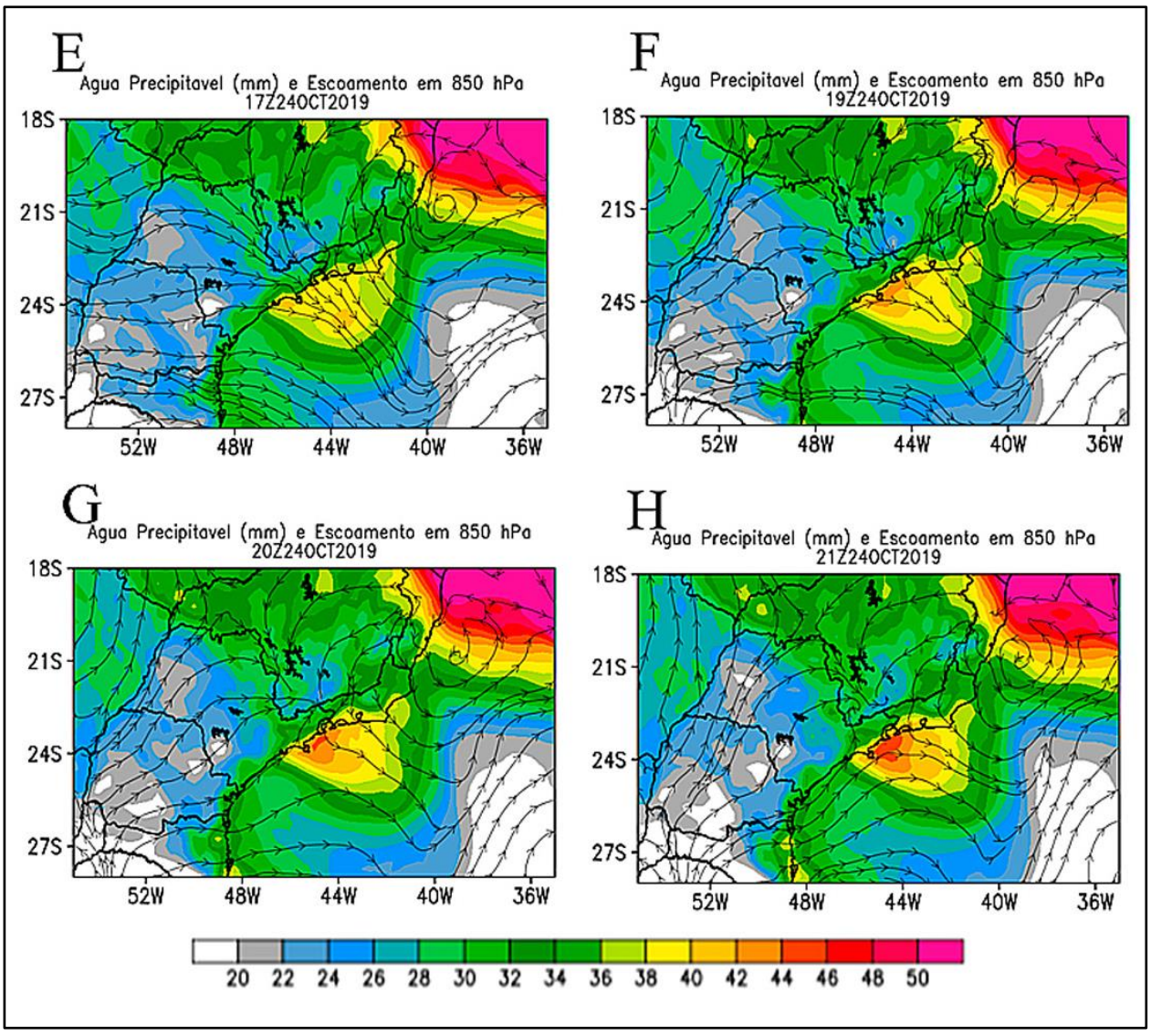

Figure 3 – Synoptic fields at 17:00, 19:00, 20:00, and 21:00 UTC on October 24th, 2019. (A-D) jets at 250 hPa (m s^{-1}; colored), streamlines at 250 hPa (m s^{-1}), and mass divergence at 250 hPa (104 s^{-1}; in yellow), (E-H) precipitable water (mm; colored), wind vectors at 850 hPa (m s^{-1}; in black, with arrows), (I-L) moisture convergence at 850 hPa (106 g $kg^{-1}s^{-1}$; colored), and wind vectors at 850 hPa (m s^{-1})

Conclusion

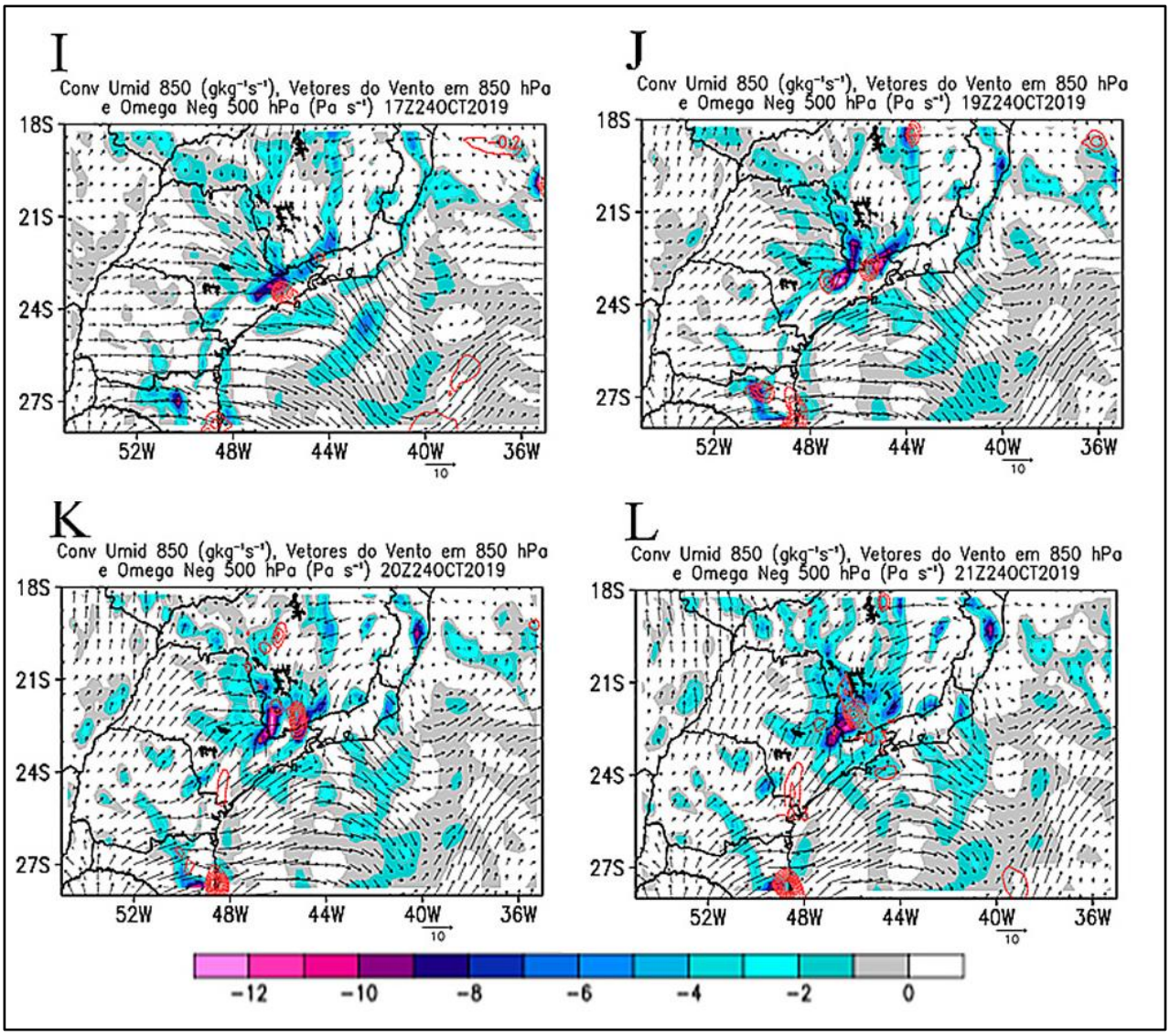

Source: Author's (2019)

Figures 3 I-L show moisture convergence at 850 hPa in phase with upper troposphere divergence (Figures 3 A-D). These two processes coupled, led to favorable atmospheric conditions for rising humid air, generating stormy conditions in SP and south MG. We can also see that these coupled processes migrated from SP at 17:00 UTC (Figure 3 I), towards south MG in the following hours (Figures 3 J-L), when the convective system propagated from SP to south MG (which will be discussed later in Figure 7). In short, mass divergence at 250 hPa lifted air, which in turn, was aided by moisture supplies through moisture convergence at 850 hPa, in this specific case.

Presence of airlifting mechanisms and thermally unstable humid air (Ahrens and Henson, 2018; Ynoue *et al*., 2017) are important conditions for cloud and storm formation. In the case of SRS thunderstorm, it was characterized by a humid atmosphere between 850-800 hPa, so air parcels that rise from these levels carry moisture with them. Another needed condition is vertical wind shear to avoid clouds self-destruction (updrafts and downdrafts within the cloud would cancel each other). The Potential for Severity and Hail index (NOAA, 2021), jointly assesses these factors, and indicates whether environments can lead to SS. Figure 4 shows this index for the SRS storm at various times of the day, along with the regions where the six criteria used to calculate the index were satisfied (in orange). Figure 4 also shows the vertical wind shear criterion in layer 6 at 0 km (550 - 1000 hPa), between 10 m s^{-1} and 20 m s^{-1} (cross-hatched section), since shear from 10 m s^{-1} supported storm formation with single cells (Markowski and Richardson, 2011), and atmospheric instability, indicated by the CAPE (colored lines), which is important for understanding storm thermodynamics, even though it was not included as a variable in the six index criteria.

Figure 4 – Potential for Severity and Hail Index (NOAA, 2021): solid orange area indicates the simultaneous occurrence of six criteria used to calculate the index at 17:00, 19:00, 20:00, and 21:00 UTC, on October 24th, 2019 (see section 2.2 for more details). Vertical wind shear > 10 m s^{-1}, calculated between the 550 hPa and 1000 hPa (m s^{-1}; black hatched part), and CAPE (J kg^{-1}; solid lines), are also shown

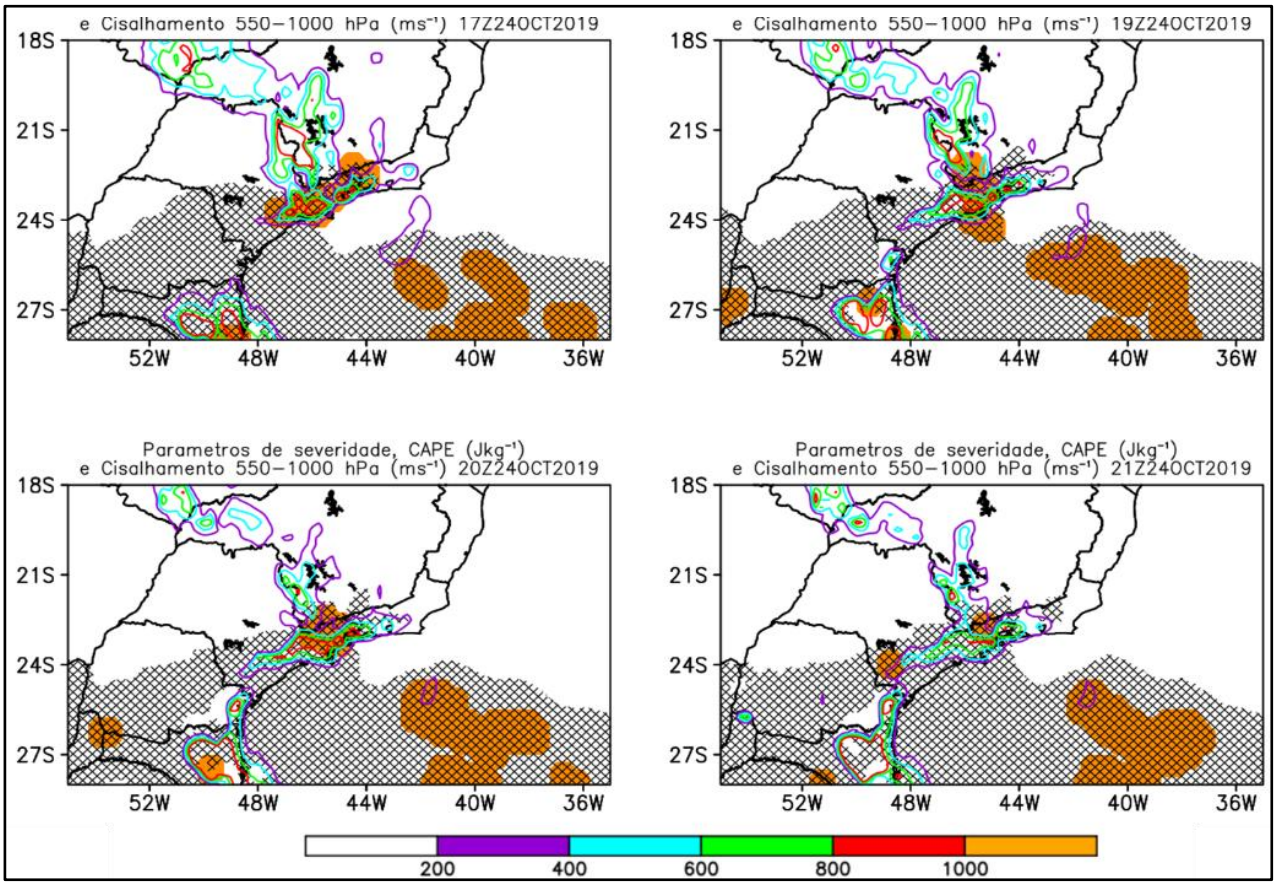

Source: Author's (2019)

The thermodynamic environment in which the SRS thunderstorm formed is represented by the SkewT-LogP diagram built from the ERA5 reanalysis data (Figure 5A), which could have shown some profile differences if radiosondes had been used in the region. Some instability indices e.g., the K and TT indices can be obtained from the information in this diagram (further details on calculating and interpreting these indices are given in Ferreira and Reboita, 2020). The K index was 35, and the TT index was 50, indicating the atmospheric potential for forming scattered storms.

Figure 5 – A. Thermodynamic conditions at 19:00 UTC on October 24th, 2019, at the grid point representing the SRS(MG) coordinates (22.24ºS; 45.68ºW). The blue line in the SkewT-LogP diagram indicates the dew point temperature (Td), the black line indicates the ambient temperature (T), and the dashed red line indicates the temperature of the air parcels (Tp) forced to ascend from the surface. LCL is the lifting condensation level. Figure 5A shows wind intensity and direction in the atmospheric layers via the barbs located on the right side of the diagram. Figure 5B shows a scatterplot diagram for vertical wind shear in the layer between the 6-0 km (m s-1; vertical axis), and CAPE (J kg-1; horizontal axis). The black lines indicate the dimensionless Richardson number. The colored dots correspond to 15:00 to 20:00 UTC on October 24th, 2019, for the grid points of the region indicated in blue, in the inner panel of the map of southeast Brazil

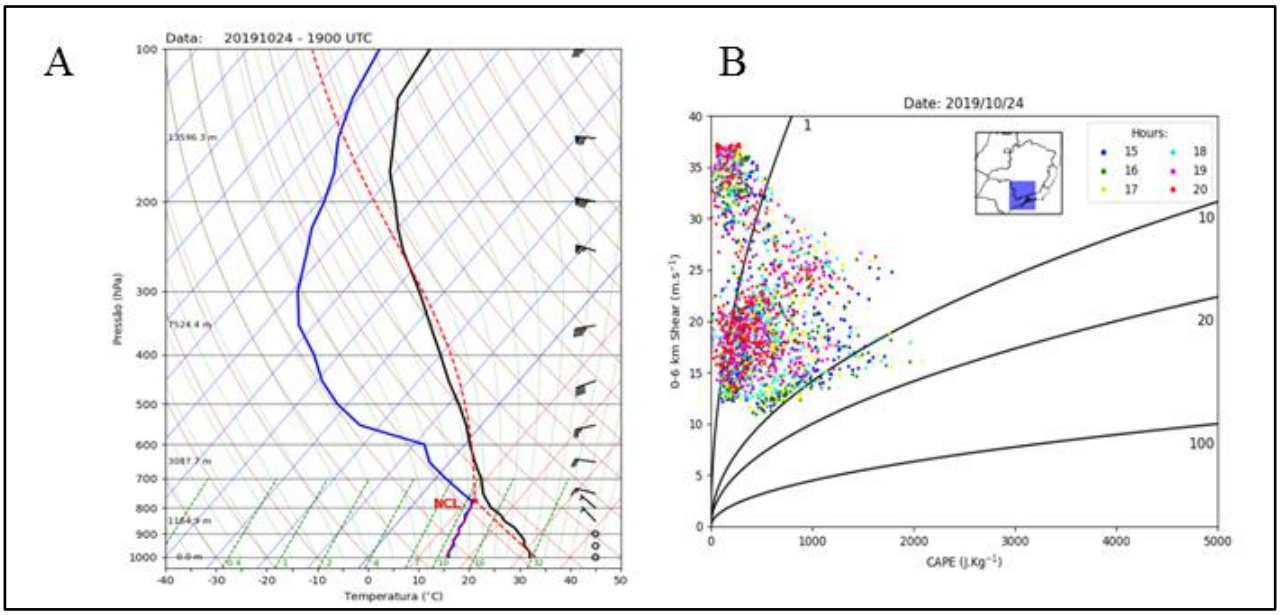

Fonte: Author's (2019)

The thermodynamic environment in that SRS thunderstorm had its genesis can be described by the SkewT-LogP diagram (Figure 5A). From the ambient temperature (T) curve in black and the dew point temperature (Td) curve in blue, it is verified that the troposphere is humid in a shallow layer and close to the 850-800 hPa level, in the region of the lifting condensation level by lifting. The distance between the T and Td curves at the other levels is an indication of drier air in the troposphere. The area between the surveyed plot path (Tp - dashed red line), and

the T curve, is equivalent to the CINE, when the plot line is to the left of the T line. In contrast, when the Tp line is to the right of the T line, this is equivalent to CAPE. In Figure 5A the CINE is -209.46 kg^{-1} according to a portion rising from the surface. The more negative the CINE value, the more difficult convective initiation becomes. The CAPE value was approximately 468.86 J kg^{-1}, according to a portion rising from the surface. The CAPE area is related to the storm's updraft. We can see that the storm in SRS had a low CAPE value, with spontaneous convection level (NCE), at approximately 650 hPa, while the equilibrium level (NE), was at about 300 hPa. This low CAPE characteristic supports the idea that vertical shear was important for forming an intense convective system. However, other factors may have been at play, i.e., dry air at levels above the lifting condensation level - LCL (Weisman and Klemp, 1986; Hassan *et al*., 2017). According to Weisman and Klemp (1986), dry atmospheres cause water droplet evaporation or ice sublimation, leading to air cooling, and consequently, subsident cold air current formation. These convective scale movements are associated with strong surface winds and are important for forming gust fronts that form new convective cells.

Figure 5B shows the BRN to assess the storm's type by synthesizing thermodynamic and dynamic information. The figure is a scatterplot between vertical wind shear between 6-0 km, and the CAPE. At 19:00 and 20:00 UTC the CAPE was less than 1000 J kg^{-1}, and vertical wind shear was around 15-20 m s^{-1} (higher point concentrations in the scatter plot). Although CAPE does not have conducive values for SS formation (Ferreira and Reboita, 2020), according to Figure 5A, vertical wind shear seemed to be important in maintaining the air currents inclination. In fact, the BRN, which ranged from 1 to 10 (shown in black in Figure 5B), even quite low, was indicative of multicellular storms (Markowski and Richardson, 2011), thus triggering a synoptic environment conductive to the storm. This corroborates the synoptic analysis discussed at the beginning of this section. The multicellular storm that passed through SRS on October 24th, 2019, resulted from dynamic and thermodynamic responses from atmospheric characteristics in southern MG. In

terms of dynamics, upper-level divergence and low-level moisture convergence destabilized the environment. The storm became severe due to vertical wind shear and drier air above the LCL, even with low CAPE values, since both factors lead to more intense downdrafts, and consequently, wind front propagation and new cells formation.

We can conclude that upper-level divergence and moisture convergence, shown in Figure 3, resulted in dynamic forcing for air ascending to the NCE, overcoming convective inhibitions imposed by the CINE (Figure 5A). Storm severity was offset by vertical wind shear in the absence of higher CAPE values, while drier air at mid-levels produced downdrafts and stronger wind fronts.

3.2 Physical Characteristics of the Storm

Figure 6 (left) shows the spatial distribution of the TWV-TIR temperature difference between 18:00 and 22:00 UTC. There was a northwest-southeasterly band of clouds that intensified over time to positive differences (> +1 K) between 20:00 and 21:00 UTC. During this period, the IN and NS lightning rates increased dramatically from 636 IN (79 NS), at 18:00 UTC, to 2922 IN (322 NS) at 20:00 UTC (when hail first precipitated) (Figures 6 B, D, F, and H). These results corroborate with Machado *et al*. (2009)'s study, where positive brightness temperature differences are associated with higher lightning rates. Positive brightness temperature differences suggest deep topped clouds, which extend beyond the tropopause, and which have lots of ice. Intense updrafts and ice at the top of clouds charge colliding hailstones (Jayaratne *et al*., 1983). Colliding ice crystals and soft hail, in the presence of supercooled water in regions with strong updrafts, are fundamental for lightning formation (Reynolds *et al*. 1957).

Figure 6 – Brightness temperature difference (K) between the water vapor channel (TWV, 6.5 μm), and the infrared channel (IRR, 10.7 μm) (TWV-TIR, colored region) on 24th, October 2019 at (A) 1800, (C) 1900, (E) 2000, (G) 2100, and (I) 2200 UTC. (B, D, F, H, and J), intra-cloud (black open circle), and cloud-ground (blue cross) lightning distribution

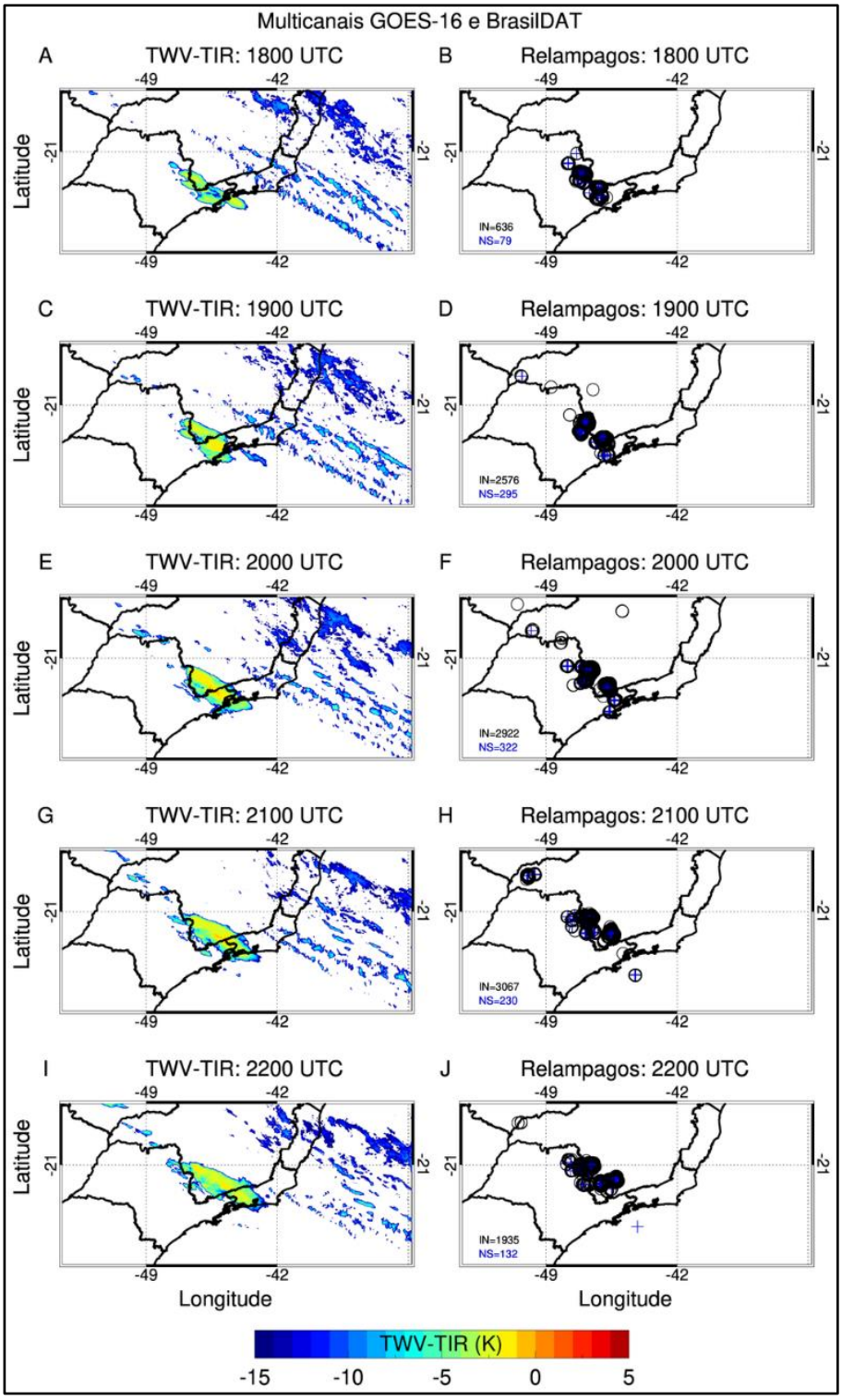

Source: Author's (2019)

Figure 7 – Constant Altitude Plan Position Indicator (CAPPI) of reflectivity (dBZ) in 3 km high for October 24, 2019 between 15:20 and 21:20 UTC from the radar of São Roque (SP). The red square represents the delimitation of the area of the storm that was tracked manually

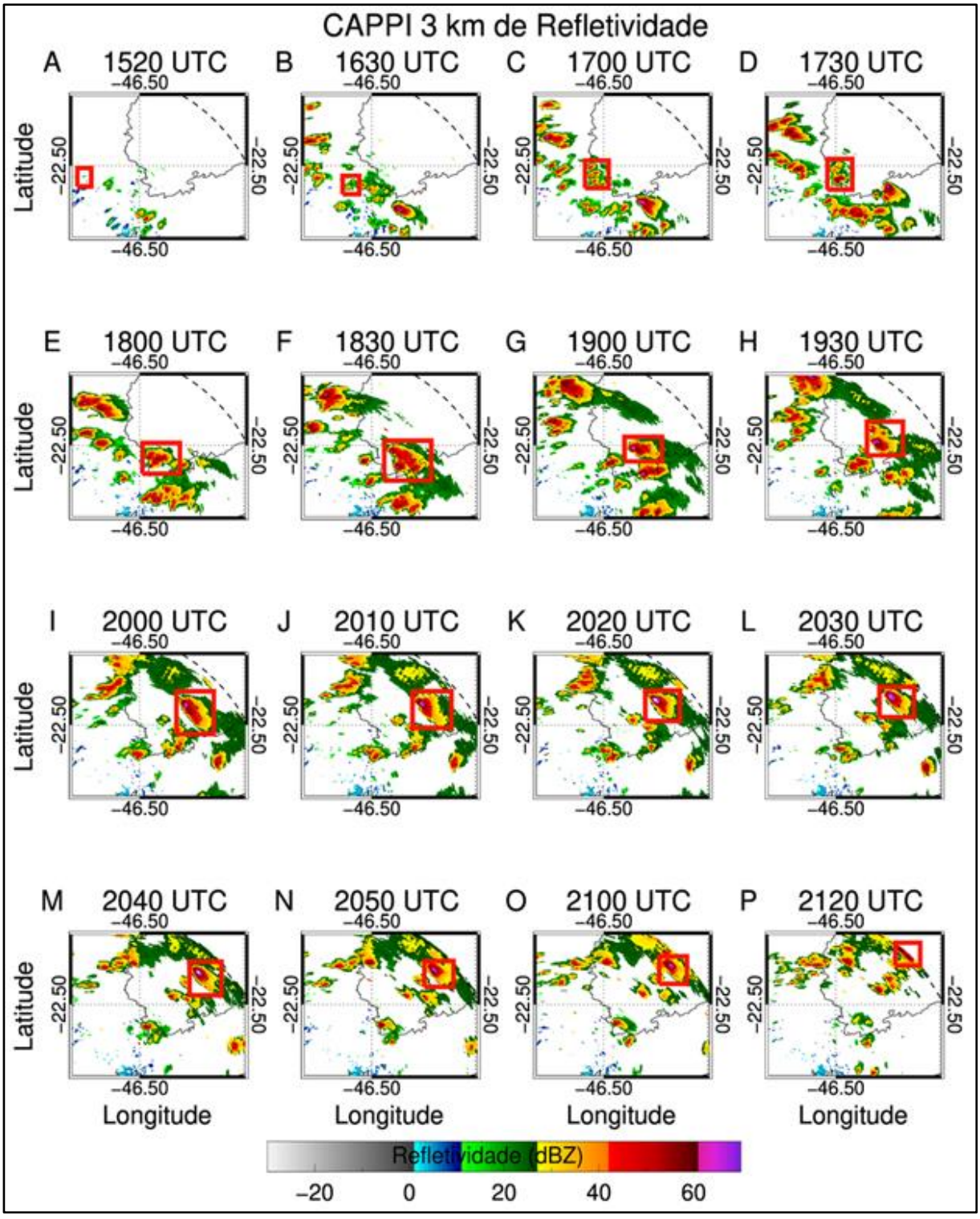

Source: Author's (2019)

Figure 7 shows the CAPPI reflectivity variable at 3 km height. The storm entered the radar zone at 15:20 UTC and was monitored until 21:20 UTC (6 h), when it moved out of range (> 240 km from the radar center) (Figure 7P). The thunderstorm that reached SRS city was formed of intense local multicellular convective cells (> 45 dBZ), confirming the BRN result, but which then converted into a single large convective cell. Between 20:00 and 21:00 UTC (Figures 7 I-O), the thunderstorm showed convective cells with reflectivity above 60 dBZ. Between 20:20 and 20:40 UTC the reflectivity values exceeded 65 dBZ. Since reflectivity depends on hydrometeors diameter raised to the sixth power (Rinehart, 2010), the results indicate that large ice particles existed at this moment.

Figure 8 shows the time evolution of lightning and the precipitation parameters of the thunderstorm. The tracking and calculation of the parameters of the storm considered that area containing pixels with reflectivity above 20 dBZ in the region defined by the square shown in Figure 7. For identification of hail, we used those radar images closest to the observation of hail on surface. The VIL and DVIL parameters gradually increased as the storm intensified (Figure 8A). Both variables reached maximum (11 kg m^{-2} and 0.8 g m^{-3}), before hail precipitated at 19:40 UTC, and decreased (6 kg m^{-2} and 0.5 g m^{-3}), at the beginning of the event at 20:00 UTC, and then increased again, reaching a second maximum during the event at 20:20 UTC, at approximately 14 kg m^{-2} and 1.0 g m^{-3}, respectively. The intense hailstone production and subsequent increase in electrical activity are typical of SS. Abrupt changes in the VIL and DVIL variables are strong indicators of strengthening or decaying storm updrafts. The VIL and DVIL values reported in this study were lower than Abreu *et al*. (2020) (46 kg m^{-2} and 3.3 g m^{-3}), and lower than SS DVIL values, as suggested by Gomes and Held (2004) (> 2.3 g m^{-3}). Although these results were relatively lower, they do indicate that combined dynamic forcing from vertical wind shear (Figure 5B), and moderate microphysics values, generated a local SS that severely impacted the population.

Figure 8 – Time evolution: (a) total intra-cloud lightning (dashed black curve, lightning/10 min), and cloud-ground lightning (solid black curve, lightning/10 min), Echo Top of 20 dBZ (solid blue curve, km), storm area (solid orange curve, km²), and maximum reflectivity (solid red curve, dBZ), and (b) vertically integrated liquid water content - VIL (solid black curve, kg/m^2), VIL - DVIL density (solid blue curve, g/m^{-3}), the Waldvogal height – AW (solid orange curve, km), and 35 dBZ Eco Top (solid red curve, km), for the storm on October 24th, 2019. The red dashed line marks the time when hail began to fall

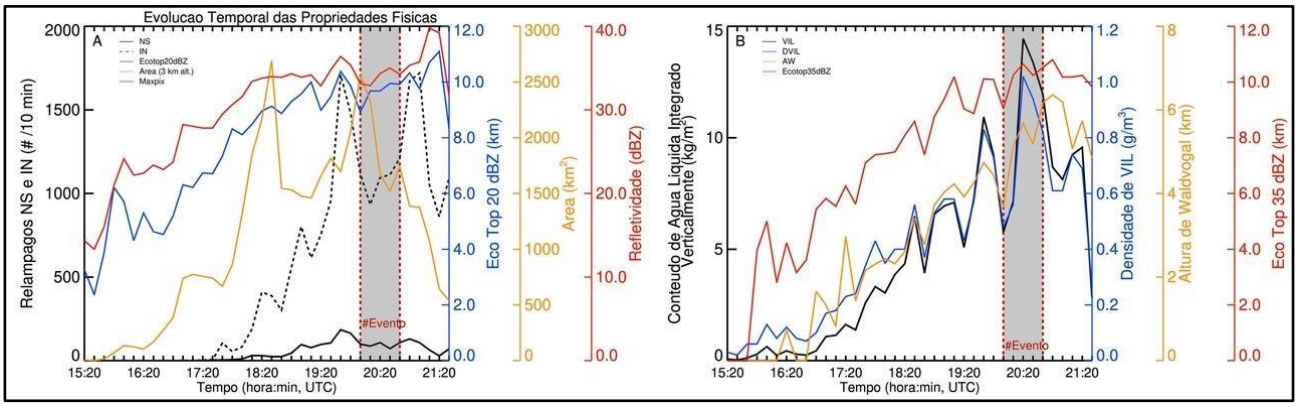

Source: Author's (2019)

Lightning peak occurs approximately 20 minutes before hail reaches surface (Figure 8A) with 1600 IN and 200 NS lightning in a 10-minute interval. This total lightning peak (IN and NS), preceding the severe weather event is similar to the Lightning Jump (Goodman *et al*., 1988; Schultz *et al*., 2011). This phenomenon occurs from rapid updraft intensifications, associated with strong convections within the storm. Condensation, associated with rapid updraft velocity intensifications in the clouds, help form ice crystals, that form larger ice particles when they collide (i.e., soft hail and hail), and these collision rates define the electrical structure of the cloud, and strongly influence electrical discharges (Sperling, 2018). When updraft flows weaken, or cannot support the weight of the ice particles, they fall in the form of precipitation. Since hail and soft hail are large

particles, they may not completely melt into raindrops, and thus fall to the ground in their solid phase.

The AW parameter can also be analyzed to determine ice layer thickness inside the cloud. It is defined as the difference between the EchoTop at 45 dBZ and the height of the isotherm at 0°C. According to Waldvogel *et al*. (1979), when AW value exceeds 1.4 km, hail within the cloud grows and falls to the surface. Therefore, AW is used to estimate hail in storm cells. Figure 8B shows that AW exceeded 6 km at the most intense phase, indicating that hail had grown sufficiently to precipitate. The first echo at reflectivity ≥ 35 dBZ was detected shortly before 16:00 UTC (Figure 8B). From this time forward, the storm size continued to grow, showing precipitation particles increasing in both size and number, further suggesting intense updrafts through the mixed phase region, favoring large hail particle formation. As the system evolved to the dissipative state, the VIL and DVIL variables decreased, probably because hail particles had fallen to the surface. Despite these reduced variables, we can see that the storm's size reduced soon after hail fell (Figure 8B), but because the storm had left the radar zone we could not verify if it had totally dissipated.

Figure 9 shows two vertical cross-sections of the thunderstorm at 20:00 UTC, representing the same moment that hail was registered on surface. Figure 9A shows that the system reduced in size, and had a small core with more intense reflectivity above 60 dBZ, suggesting the existence of large ice particles. Also consistent with the presence of ice, Figure 9B shows a high IN rate (1016 lightning/10 min), and a high NS rate (99 lightning/10 min), near the moderate reflectivity region (55 dBZ), located to the right of where hail had fallen (in pink, reflectivity > 60 dBZ). Regarding low-level flow and system displacement from the southwest to the northeast, maximum lightning rates occurred at the rear of the storm. Most lightning was concentrated in a region with moderate (> 55 dBZ) reflectivity (Figures 9B-D), which corroborates other studies on compact storms (Mattos *et al*., 2017, de Abreu *et al*., 2020). These results show that lightning

occurred after hail had already been detected by radar, where the convective center descended within the storm. These results corroborate with Goodman *et al*. (1988), who showed that intra-cloud lightning followed hail detection by radar, during a period of rapid vertical cloud development, when storms reach maximum height, and when the first cloud-to-ground lightning occurred in the moment that the maximum reflectivity descended inside the cloud. The collapse or weakening of the updrafts probably produced conditions for increased collision rates between ice particles, favoring dielectric strength disruption of the air inside the cloud, consequently forming lightning at that moment. Additionally, these results show that the microphysical and dynamic conditions of this particular storm efficiently promoted ice formation and electrical activity, even though the most intense area of the system was compact and localized.

We can see that the system had a 16 km vertical extension, with a more intense core (> 60 dBZ, in pink color), and a 5 km horizontal extension, reaching 8 km, upon analyzing the vertical section (Figures 9C and D). This high reflectivity region between the cloud base (2 km), and the mixed storm phase, indicates hail inside the storm cloud. This study used the layer between the 0°C and -15°C isotherms inside the clouds as the mixed phase region, employing a methodology similar to Mattos *et al*. (2016), to study the vertical structure of cloud microphysics via radar data. This extensive vertical column that entered the mixed cloud phase is commonly observed in storms with strong updrafts and efficient ice particle production. Mattos *et al*. (2017), de Abreu *et al*. (2020), and Lhermitte and Williams (1985) observed and discussed maximum reflectivity close to the -16ºC isotherm, known as the balance level, where the average terminal velocity of the hail particles equals the velocity of the updrafts, favoring suspended hail formation at the top of updrafts.

Figure 9 – A. CAPPI reflectivity (dBZ) at 3 km; B. Lightning distribution from the ENTLN network between 20:00 and 20:10 UTC (IN: open circles, and NS: blue crosses), and reflectivity radar contours (30 and 55 dBZ); C. vertical reflectivity cut (in dBZ), and lightning rates (ENTLN) for images closest to when hail first fell (2000 UTC); D. vertical reflectivity cut (in dBZ), and lightning rates (ENTLN) for images closest to when hail first fell (2000 UTC); The vertical section location from Figure 9C (Figure 9D) is represented by the blue line (black), in Figures 9A and 9B

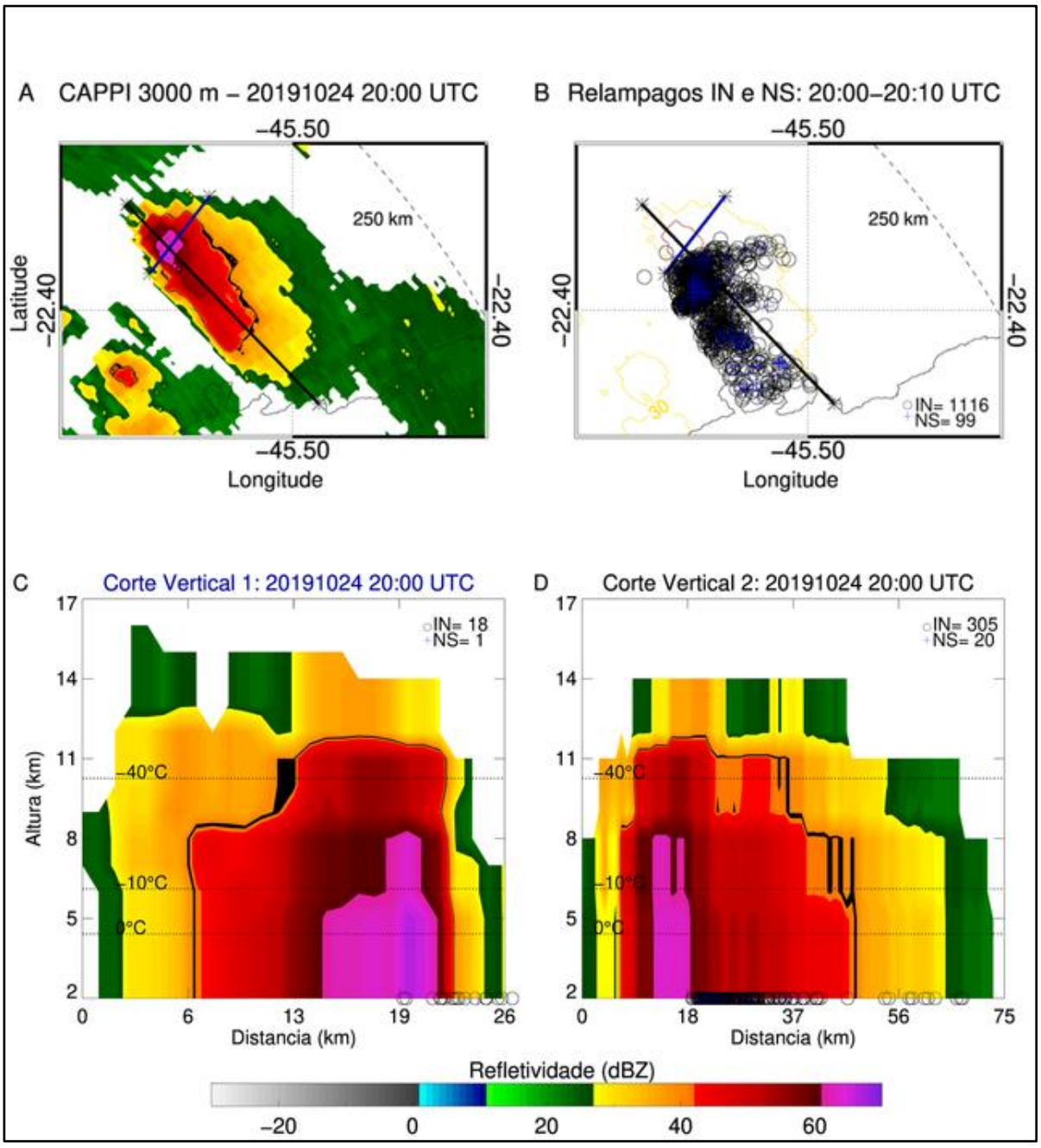

Source: Author's (2019)

4 CONCLUSION

This study analyzed the development of a thunderstorm that produced hail in Santa Rita do Sapucaí (SRS) city (MG) in Brazil, in the afternoon of October 24th, 2019. This study was the first to analyze a hailstorm in SRS. The main results obtained are listed below.

The synoptic analysis indicated that mass divergence in the upper troposphere combined with low-level moisture convergence providing synoptic scale upward vertical movements in the studied area between 20:00 and 21:00 UTC (17:00 and 18:00 local time), led to SS formation, according to the Potential for Severity and Hail index.

From a mesoscale perspective, the instability index analyses did not show high CAPE, K, and TT values, a problem which may have resulted from using reanalysis. However, BRN indicated that vertical wind shear between 0 and 6 km was an important “factor” for maintaining the storm. Furthermore, upper-level air, drier than that in the LCL, may have contributed to storm formation by providing evaporative cooling, and consequently, generating subsidence currents. These currents form surface wind fronts that act as mechanisms for lifting air and generating new storm cells. In fact, as per the theoretical diagram from Vasquez (2017), BRN < 10 is indicative of multicellular storms with synoptic triggers.

Regarding the physical aspects of the storm:

a) the multichannel water vapor and infrared analysis showed deep clouds (positive differences) with high lightning rates, showing that there was intense ice production;
b) weather radar data analysis revealed that the storm was small, with isolated precipitating nuclei, that developed rapidly, and lasted for quite some time (15:20 to 21:20 UTC);
c) the 35 dBZ Echo top showed a gradual increase throughout the storm's life cycle, indicating ice particle growth, while VIL and DVIL showed

rapid decreases at the beginning of hail precipitation, which later increased. Similarly, the ice-producing storm core was compact (< 5 km), and showed a well-developed internal cloud structure with high reflectivity (> 60 dBZ) reaching up to 8 km in the mixed cloud phase.

These results show that combined electrical activity and internal storm structure parameters are fundamental for estimating storm impacts.

The storm that hit Santa Rita do Sapucaí had very negative impacts on society. This highlights the need for, and the importance of monitoring severe weather events over short/very short time scales, not only for the residents of SRS, but for all of Brazil.

ACKNOWLEDGMENTS

The authors would like to thank ECMWF, CLIMATEMPO, the Department of Airspace Control (DECEA), the Center for Weather Forecasting and Climate Studies (CPTEC) from the National Institute for Space Research (INPE) for providing the data used in this study. We would also like to thank CNPQ, FAPEMIG, and CAPES (financial code 001) for their financial support.

REFERENCES

ABREU, E. X.; MATTOS, E.; SPERLING, V. B. Caracterização das Assinaturas de Radar e da Atividade Elétrica de Relâmpagos de Tempestades com Granizo no Estado de São Paulo. **Anuário do Instituto de Geociencias**, [*s.l.*], v. 43, n. 2, p. 173-188, 2020. DOI 10.11137/2020_02_173_188. Disponível em: https://doi.org/10.11137/2020_02_173_188

AHRENS, C. D.; HENSON, R. **Meteorology today**: an introduction to weather, climate, and the environment. Boston: Cengage learning, 2018. 736 p.

ALCÂNTARA, C. R. Linha de instabilidade da Amazônia: estudo de caso e importância das características do perfil do vento na sua formação e desenvolvimento. **Ciência e Natura**, Santa Maria, v. 33, n. 2, p. 197-226, 2011. DOI 10.5902/2179460X9370. Disponível em: https://doi.org/10.5902/2179460X9370

ASHFAQ, M.; CAVAZOS, T.; REBOITA, M. S.; TORRES-ALAVEZ, J. A.; IM, E. S.; OLUSEGUN, C. F.; ALVES, L.; KEY, K.; ADENIYI, M. O.; TALL, M.; SYLA, M.B.; MEHMOOD, S.; ZAFAR, Q.; DAS, S.; DIALLO, I.; ERIKA, C.; GIORGI, F. 2020. Robust late twenty-first century shift in the regional monsoons in RegCM-CORDEX simulations. **Climate Dynamics**, [*s.l.*], v. 31, n. 16, p. 130-175, 2020. DOI: 10.1007/s00382-020-05306-2. Disponível em: https://doi.org/10.1007/s00382-020-05306-2

BARNES, G. Severe local storms in the tropics. *In*: DOSWELL, C. A. (Ed.). **Severe Convective Storms**. Boston, MA: American Meteorological Society p. 359–432, 2001. DOI 10.1007/978-1-935704-06-5_10. Disponível em: https://doi.org/10.1007/978-1-935704-06-5_10

BEAL, A.; HALLAK, R.; MARTINS, L. D.; MARTINS, J. A.; BIZ, G.; RUDKE, A. P.; TARLEY, C. R. Climatology of hail in the triple border Paraná, Santa Catarina (Brazil) and Argentina. **Atmospheric Research**, [*s.l.*], v. 234, e104747, 2020. DOI 10.1016/j.atmosres.2019.104747. Disponível em: https://doi.org/10.1016/j.atmosres.2019.104747

BEDKA, K. M. Overshooting cloud top detections using MSG SEVIRI Infrared brightness temperatures and their relationship to severe weather over Europe. **Atmospheric Research**, [*s.l.*], v. 99, n. 2, p. 175-189, 2011. DOI 10.1016/j.atmosres.2010.10.001. Disponível em: https://doi.org/10.1016/j.atmosres.2010.10.001

CECIL, D. J.; BLANKENSHIP, C. B. Toward a global climatology of severe hailstorms as estimated by satellite passive microwave imagers. **Journal of Climate**, [*s.l.*], v. 25, n. 2, p. 687-703, 2012. DOI 10.1175/JCLI-D-11-00130.1. Disponível em: https://doi.org/10.1175/JCLI-D-11-00130.1

ESTADO DE MINAS. Chuva de granizo arrasa cidade do Sul de Minas; uma pessoa morre. **ESTADO de MINAS**, Belo Horizonte, 2019 Disponível em: https://www.em.com.br/app/noticia/gerais/2019/10/24/interna_gerais,1095636/chuva-de-granizo-arrasa-cidade-do-sul-de-minas-uma-pessoa-morre.shtml. Acesso em: 11 fev. 2021.

FERREIRA, C.; REBOITA, M.S. **Índices de instabilidade: o que são e para que servem?**. São Paulo: Câmara Brasileira do Livro, 2020. 80 p.

GÁLVEZ, J. M. SANTAYANA, N. 2019. **GR02T: Potential for Severity and Hail**. Disponível em: https://www.wpc.ncep.noaa.gov/international/wng/DOC/GR02T/ Acesso em: 21 mar. 2021

GATTI, E. C. 2019. **Estudo de sistemas convectivos de mesoescala em Santa Catarina no período primavera/verão 2018-2019.** 2019. 91p. (Trabalho de Conclusão de Curso) – Programa de Graduação em Meteorologia, Universidade Federal de Santa Catarina, 2019.

GOMES, A. M.; HELD, G. Determinação e avaliação do parâmetro densidade VIL para alerta de tempestades. *In*: XIII CONGRESSO BRASILEIRO DE METEOROLOGIA, 2, Fortaleza, 2004. **Resumos** [...]. Fortaleza: UFC, 2004, p. 72-87.

GOODMAN, S. J.; BUECHLER, D. E.; WRIGHT, P. D.; RUST, W. D. Lightning and precipitation history of a microburst-producing storm. **Geophysical research letters**, [*s.l.*], v. 15, n. 11, p. 1185-1188, 1998. DOI 10.1029/GL015i011p01185. Disponível em: https://doi.org/10.1029/GL015i011p01185

GREENE, D. R.; CLARK, R. A. Vertically integrated liquid water - A new analysis tool. **Monthly Weather Review**, [*s.l.*], v. 100, n. 7, p. 548-552, 1972. DOI 10.1175/1520-0493(1972)100<0548:VILWNA>2.3.CO;2. Disponível em: https://doi.org/10.1175/1520-0493(1972)100<0548:VILWNA>2.3.CO;2

HASSAN, V. V.; FRANÇA, J. R. A.; MENEZES, W. F.; PERES, L. F. 2017. Características meteorológicas do ambiente sinótico e de meseoescala associadas ao evento de tornado na cidade de Xanxerê – SC, em abril de 2015. **Anuário Igeo**, [*s.l.*], v. 40, n. 3, p. 131-138, 2017. DOI 10.11137/2017_3_131_138. Disponível em: http://dx.doi.org/10.11137/2017_3_131_138

HERSBACH, H.; BELL, B.; BERRISFORD, P.; HIRAHARA, S.; HORÁNYI, A.; MUÑOZ-SABATER, J.; NICOLAS, J.; PEUBEY, C.; RADU, R.; SCHEPERS, D.; SIMMONS, A.; SOCI, C.; ABDALLA, S.; ABELLAN, X.; BALSAMO, G.; BECHTOLD, P.; BIAVATI, G.; BIDLOT, J.; BONAVITA, M.; CHIARA, G. de.; DAHLGREN, P.; DEE, D.; DIAMANTAKIS, M.; DRAGANI, R.; FLEMMING, J.; FORBES, R.; FUENTES, M.; GEER, A.; HAIMBERGER, L.; HEALY, S.; HOGAN, R. J.; HÓLM, E.; JANISKOVÁ, M.; KEELEY, S.; LALOYAUX, P.; LOPEZ, P.; LUPU, C.; RADNOTI, G.; ROSNAY, P. de; ROZUM, I.; VAMBORG, F.; VILAUME, S.; THÉPAUT, J. N. The ERA5 global reanalysis. **Quarterly Journal of the Royal Meteorological Society**, [*s.l.*], v. 146, n. 730, p. 1999-2049, 2020. DOI 10.1002/qj.3803. Disponível em: https://doi.org/10.1002/qj.3803

HOLTON, J.R. **Introduction to Dynamic Meteorology**. 4th. ed. Amsterdam: Elsevier, 2004. 535 p.

IBGE – Instituto Brasileiro de Geografia e Estatística. **Censo demográfico 2010:** população de Santa Rita do Sapucaí. [*s.l.*], 2020. c2017. Disponível em: https://cidades.ibge.gov.br/brasil/mg/santa-rita-do-sapucai/panorama. Acesso em: 11 dez. 2020.

INATEL – **Instituto Nacional de Telecomunicações**. 2020. Disponível em: https://www.inatel.br/home/santa-rita-do-sapucai. Acesso em: 11 fev. 2021.

INTERNATIONAL DESKS. **Weather Prediction Center**. [*s.l.*], 2020 Disponível em: https://www.wpc.ncep.noaa.gov/international/wng/DOC/GR02T/. Acesso em: 06 dez. 2020.

JAYARATNE, E. R.; SAUNDERS, C. P. R.; HALLETT, J. Laboratory studies of the charging of soft-hail during ice crystal interactions. **Quarterly Journal of the Royal Meteorological Society**, [*s.l.*], v. 109, n. 461, p. 609-630, 1983. DOI 10.1002/qj.49710946111. Disponível em: https://doi.org/10.1002/qj.49710946111

JOHNS, R. H.; DOSWELL III, C. A. Severe local storms forecasting. **Weather and Forecasting**, [*s.l.*], v. *7*, n. 4, p. 588-612, 1992. DOI 10.1175/1520-0434(1992)007<0588:SLSF>2.0.CO;2. Disponível em: https://doi.org/10.1175/1520-0434(1992)007<0588:SLSF>2.0.CO;2

JORNAL G1. 2019. **Mulher morre após queda de árvore durante chuva em Santa Rita do Sapucaí, MG**. Disponível em: https://g1.globo.com/mg/sul-de-minas/noticia/2019/10/24/mulher-morre-apos-queda-de-arvore-durante-chuva-em-santa-rita-do-sapucai-mg.ghtml. Acesso em: 11 fev. 2021.

KNEIB, R. O. **Estudo observacional das linhas de instabilidade no Estado do Paraná**. 2004. 128p. Dissertação (Mestrado em Meteorologia) – Programa de Pós-graduação em Meteorologia, Instituto Nacional de Pesquisas Espaciais, Dissertação de Mestrado, 2004

LHERMITTE, R.; WILLIAMS, E. Thunderstorm electrification: A case study. **Journal of Geophysical Research: Atmospheres**, [*s.l.*], v. 90, d. 4, p. 6071-6078, 1985. DOI 10.1029/JD090iD04p06071. Disponível em: https://doi.org/10.1029/JD090iD04p06071

MACHADO, L. A.; LIMA, W. F.; PINTO JR, O.; MORALES, C. A. Relationship between cloud-to-ground discharge and penetrative clouds: A multi-channel satellite application. **Atmospheric Research**, [*s.l.*], v. *93*, n. 1-3, p. 304-309, 2009. DOI 10.1016/j.atmosres.2008.10.003. Disponível em: https://doi.org/10.1016/j.atmosres.2008.10.003

MARENGO, J. A.; AMBRIZZI, T.; ALVES, L. M.; BARRETO, N. D. J. D. C.; REBOITA, M.; RAMOS, A. 2020. Changing Trends in Rainfall Extremes in the Metropolitan Area of São Paulo: causes and impacts. **Frontiers Climate**, [*s.l.*], v. 2, n. 3, p. 1-13, 2020. DOI 10.3389/fclim.2020.00003. Disponível em: 10.3389/fclim.2020.00003

MARKOWSKI, P.; RICHARDSON, Y. **Mesoscale meteorology in midlatitudes.** vol. 2. Oklahoma: John Wiley e Sons, 2011. 430 p.

MARTINS, J. A.; BRAND, V. S.; CAPUCIM, M. N.; FELIX, R. R.; MARTINS, L. D.; FREITAS, E. D.; GONÇALVES, F. L. T.; HALLAK, R.; SILVA DIAS, M. A. F.; CECIL, D. J. Climatology of destructive hailstorms in Brazil. **Atmospheric Research**, [*s.l.*], v. 184, p. 126-138, 2017. DOI 10.1016/j.atmosres.2016.10.012. Disponível em: https://doi.org/10.1016/j.atmosres.2016.10.012

MATTOS, E. V.; MACHADO, L. A. T.; WILLIAMS, E. R.; Albrecht, R. I. 2016. Polarimetric radar characteristics of storms with and without lightning activity,J. Geophys. **Research: Atmospheres**, [*s.l.*], v. 12, n. 23, p. 201-220, 2016: DOI 10.1002/2016JD025142. Disponível em: https://doi.org/10.1002/2016JD025142

MATTOS, E. V.; MACHADO, L. A.; WILLIAMS, E. R.; GOODMAN, S. J.; BLAKESLEE, R. J.; BAILEY, J. C. Electrification life cycle of incipient thunderstorms. **Journal of Geophysical Research: Atmospheres**, [*s.l.*], v. *122*, n. 8, p. 4670-4697, 2017. DOI 10.1002/2016JD025772. Disponível em: https://doi.org/10.1002/2016JD025772

MATTOS, E. V.; REBOITA, M. S.; LLOPART, M. P.; ENORÉ, D. P. Análise Sinótica e Caracterização Física de uma Tempestade Intensa Ocorrida na Região de Bauru-SP. **Anuario do Instituto de Geociencias**, [*s.l.*], v. 43, n. 1, p. 85-106, 2020. DOI 10.11137/2020_1_85_106. Disponível em: http://dx.doi.org/10.11137/2020_1_85_106

MILLS, G. A.; COLQUHOUN, J. R. Objective Prediction of Severe Thunderstorm Environments: Preliminary Results Linking a Decision Tree with an Operational Regional NWP Model, **Weather and Forecasting**, [*s.l.*], v. 13, n. 4, p. 1078-1092, 1998. Disponível em: https://journals.ametsoc.org/view/journals/wefo/13/4/1520-0434_1998_013_1078_oposte_2_0_co_2.xml Acesso em: 22 de mar. 2021

MOLLER, A. R. Severe local storms forecasting. *In:* DOSWELL III, C. A. (ed). **Meteorological Monographs**. American Meteorological Society, p. 433-480, 2001. DOI 10.1007/978-1-935704-06-5_11. Disponível em: https://doi.org/10.1007/978-1-935704-06-5_11

MONCRIEFF, M. W.; GREEN, J. S. A. The propagation and transfer properties of steady convective overturning in shear. **Quarterly Journal of the Royal Meteorological Society**, [*s.l.*], v. 98, n. 416, p. 336-352, 1972. DOI 10.1002/qj.49709841607. Disponível em: https://doi.org/10.1002/qj.49709841607

MONTINI, T. L.; JONES, C.; CARVALHO, L. M. The South American low-level jet: A new climatology, variability, and changes. **Journal of Geophysical Research: Atmospheres**, [*s.l.*], v. 124, n. 3, p. 1200-1218, 2019. DOI 10.1029/2018JD029634. Disponível em: https://doi.org/10.1029/2018JD029634

NASCIMENTO, E. L. Previsão de tempestades severas utilizando-se parâmetros convectivos e modelos de mesoescala: uma estratégia operacional adotável no Brasil? **Revista Brasileira de Meteorologia**, [*s.l.*], v. 20, n. 1, p. 121-140, 2005.

NOAA. **National Oceanic and Atmospheric Administration**. 2021. Bulk Richardson Number. Disponível em: https://www.spc.noaa.gov/exper/mesoanalysis/help/help_brn.html#:~:text=Help%20%2D%20Bulk%20Richardson%20Number,lowest%20500%20m%20mean%20wind. Acesso em: 11 fev. 2021

PINHEIRO, H. R.; ESCOBAR, G. C. J.; ANDRADE, K. M. Aplicação de uma ferramenta objetiva para previsão de tempo severo em ambiente operacional. **Revista Brasileira de Meteorologia**, [*s.l.*], v. *29*, n. 2, p. 209-228, 2014. DOI 10.1590/S0102-77862014000200006. Disponível em: https://doi.org/10.1590/S0102-77862014000200006.

Portal G1 2019. Mulher morre após queda de árvore durante chuva em Santa Rita do Sapucaí, MG**.** Disponível em: https://g1.globo.com/mg/sul-de-minas/noticia/2019/10/24/mulher-morre-apos-queda-de-arvore-durante-chuva-em-santa-rita-do-sapucai-mg.ghtml. Acesso em: 18 nov 2020.

REBOITA, M. S.; GAN, M. A.; ROCHA, R. P. D.; AMBRIZZI, T. Regimes de precipitação na América do Sul: uma revisão bibliográfica. **Revista brasileira de meteorologia**, [*s.l.*], v. *25*, n. 2, p. 185-204, 2010. DOI 10.1590/S0102-77862010000200004. Disponível em: http://dx.doi.org/10.1590/S0102-77862010000200004

REBOITA, M. S.; MARIETTO, D. M. G.; SOUZA, A.; BARBOSA, M. Caracterização atmosférica quando da ocorrência de eventos extremos de chuva na região sul de Minas Gerais. **Revista Brasileira de Climatologia**, [*s.l.*], v. 21, n. 13, p. 20-37, 2017. DOI 10.5380/abclima.v21i0.47577. Disponível em: http://dx.doi.org/10.5380/abclima.v21i0.47577

REYNOLDS, S. E.; BROOK, M.; GOURLEY, M. F. Thunderstorm charge separation. **Journal of Atmospheric Sciences**, [*s.l.*], v. 14, n. 5, p. 426-436, 1957. DOI 10.1175/1520-0469(1957)014<0426:TCS>2.0.CO;2. Disponível em: https://doi.org/10.1175/1520-0469(1957)014<0426:TCS>2.0.CO;2

RINEHART, R. E. **Radar for meteorologists**. Nevada Missouri: Rinehart Publications, 2010. 482 p.

SANTOS, D. F.; REBOITA, M. S. Jatos de baixos níveis a leste dos andes: comparação entre duas reanálises. **Revista Brasileira de Climatologia**, [*s.l.*], v. *22*, n. 14, p. 423-445, 2018. DOI 10.5380/abclima.v22i0.47595. Disponível em: http://dx.doi.org/10.5380/abclima.v22i0.47595

SCHMETZ, J.; TJEMKES, S. A.; GUBE, M.; VAN DE BERG, L. 1997. Monitoring deep convection and convective overshooting with METEOSAT. **Advances in Space Research**, [*s.l.*], v. 19, n. 3, p. 433-441. DOI 10.1016/S0273-1177(97)00051-3. Disponível em: https://doi.org/10.1016/S0273-1177(97)00051-3.

SCHMIT, T. J.; GUNSHOR, M. M.; MENZEL, W. P.; GURKA, J. J.; LI, J.; BACHMEIER, A. S. Introducing the nex-generation advance baseline imager on GOES-5. **Bulletin of the American Meteorological Society**, [*s.l.*], v. 86, n. 8, p. 1079-1096, 2005. DOI 10.1175/BAMS-86-8-1079. Disponível em: https://doi.org/10.1175/BAMS-86-8-1079

SCHULTZ, C. J.; PETERSEN, W. A.; CAREY, L. D. Lightning and severe weather: A comparison between total and cloud-to-ground lightning trends. **Weather and forecasting**, [*s.l.*], v. 26, n. 5, p. 744-755, 2011. DOI 10.1175/WAF-D-10-05026.1. Disponível em: https://doi.org/10.1175/WAF-D-10-05026.1

SILVA DIAS, M. A. F. D.; GRAMMELSBACHER, E. A. A possível ocorrência de tornado em São Paulo no dia 26 de abril de 1991: um estudo de caso. **Revista Brasileira de Meteorologia**, [*s.l*], v. 6, n. 2, p. 513-522, 1991.

SILVA NETO, C. P. D. **Abordagem descritiva de topo de sistemas convectivos baseada em combinações de diferenças de temperatura de canais do METEOSAT-9 e modelo numérico**. 2014. 128p. Dissertação (Mestrado em Meteorologia) – Programa de Pós-graduação em Meteorologia, Universidade Federal de Alagoas, 2014.

SILVA, J. P. R.; REBOITA, M. S.; ESCOBAR, G. C. J. Caracterização da Zona de Convergência do Atlântico Sul em campos atmosféricos recentes. **Revista Brasileira de Climatologia**, [*s.l.*], v. 25, n. 15, p. 355-377, 2019. DOI 10.5380/abclima.v25i0.64101. Disponível em: http://dx.doi.org/10.5380/abclima.v25i0.64101

SPERLING, V. B. 2018. **Processos Físicos e Elétricos das Tempestades de Granizo na Região Sul do Brasil.** 2018. 211p. Tese (Doutorado em Meteorologia) – Programa de pós-graduação em Meteorologia, Instituto Nacional de Pesquisas Espaciais, 2018

STENSRUD, D. J.; CORTINAS JR, J. V.; BROOKS, H. E. Discriminating between tornadic and nontornadic thunderstorms using mesoscale model output. **Weather and forecasting**, [*s.l.*], v. 12, n. 3, p. 613-632, 1997. DOI 10.1175/1520-0434(1997)012<0613:DBTANT>2.0.CO;2. Disponível em: https://doi.org/10.1175/1520-0434(1997)012<0613:DBTANT>2.0.CO;2

TAVARES, J. P. N.; MOTA, M. A. S. D. Condições termodinâmicas de eventos de precipitação extrema em Belém-Pa durante a estação chuvosa. **Revista Brasileira de Meteorologia**, [*s.l.*], v. 27, n. 2, p. 207-218, 2012. DOI 10.1590/S0102-77862012000200007. Disponível em: https://doi.org/10.1590/S0102-77862012000200007

THOMPSON, R. L.; EDWARDS, R.; HART, J. A.; ELMORE, K. L.; MARKOWSKI, P. 2003: Sondagens de proximidade dentro de ambientes de supercélulas obtidas a partir do Ciclo de Atualização Rápida. **Wea. Previsão**, [*s.l.*], v. 18, p. 1243-1261, 2003.

UOL Notícias. 2019. **Chuva de granizo mata mulher e muda paisagem em cidade de MG.** Disponível em: https://noticias.uol.com.br/cotidiano/ultimas-noticias/2019/10/25/chuva-de-granizo-mata-idosa-e-muda-paisagem-em-cidade-de-mg.htm. Acesso em: 11 fev. 2021.

VASQUEZ, I. L.; ARAUJO, L.; MOLION, L. C. B.; ABDALAD, M. de ARAUJO. Historical analysis of interannual rainfall variability and trends in southeastern Brazil based on observation and remotely sensed data. **Climate Dynamics**, [*s.l.*], v. 50, n. 3-4, p. 801-824, 2017.

WALDVOGEL, A.; FEDERER, B.; GRIMM, P. Criteria for the detection of hail cells. **Journal of Applied Meteorology and Climatology**, [*s.l.*], v. 18, n. 12, p. 1521-1525, 1979. DOI 10.1175/1520-0450(1979)018<1521:CFTDOH>2.0.CO;2. Disponível em: https://doi.org/10.1175/1520-0450(1979)018<1521:CFTDOH>2.0.CO;2

WALLACE, J. M.; HOBBS, P. V. **Atmospheric science: an introductory survey**. vol. 92. Boston: Elsevier, 2006. 504 p.

WCP. **Weather Prediction Center**. 2020. ALGORITHM GFS. Domain 9: Central South America. Disponível em: https://www.wpc.ncep.noaa.gov/international/wng/09_CSA/index.shtml. Acesso em: 20 mar. 2021.

WEISMAN, M. L.; KLEMP, J. B. The structure and classification of numerically simulated convective storms in directionally varying wind shears. **Monthly Weather Review**, [*s.l.*], v. 112, n. 12, p. 2479-2498, 1984. DOI 10.1175/1520-0493(1984)112<2479:TSACON>2.0.CO;2. Disponível em: https://doi.org/10.1175/1520-0493(1984)112<2479:TSACON>2.0.CO;2

YNOUE, R. Y.; REBOITA, M. S.; AMBRIZZI, T.; SILVA, G.A da. **Meteorologia: noções básicas**. São Paulo: Oficina de Textos, 2017. 182 p.

Authorship contributions

1 – Bruna Andrelina (Corresponding Author)
Meteorologist, Master in Environment and Water Resources
https://orcid.org/0000-0001-5606-7608 • brunaandrelina@gmail.com
Contribution: Conceituação, Análise Formal, Visualização, Escrita – revisão e edição

2 – Michelle Simões Reboita
Meteorologist, PhD in Meteorology
https://orcid.org/0000-0002-1734-2395 • reboita@unifei.edu.br
Contribution: Conceituação, Análise Formal, Escrita – revisão e edição

3 – Enrique Vieira Mattos
Meteorologist, PhD in Meteorology
https://orcid.org/0000-0002-9590-3709 • enrique@unifei.edu.br
Contribution: Conceituação, Escrita – revisão e edição

4 – Bruno César Capucin
Meteorologist, Master's degree in progress in Environment and Water Resources
https://orcid.org/0000-0003-0166-6739 • brunocapucin23@gmail.com
Contribution: Visualização, Escrita – revisão e edição

5 – Larissa Helena da Costa
Graduation in progress in Computer Science
https://orcid.org/0000-0002-5437-5663 • larissacosta.1996@hotmail.com
Contribution: Conceituação, Metodologia, Visualização, Escrita-primeira redação

6 – Diego Pereira Enoré
Meteorologist, Master's in Meteorology
https://orcid.org/0000-0001-7001-0560 • diegoenore@gmail.com
Contribution: Curadoria de dados, revisão e edição

7 – Thiago Souza Biscaro
Meteorologist, PhD in Meteorology
https://orcid.org/0000-0002-2338-3871 • thiago.biscaro@inpe.br
Contribution: Curadoria de dados, revisão e edição

How to quote this article

ANDRELINA, B.; REBOITA, M. S.; MATTOS, E. V.; CAPUCIN, B. C.; COSTA, L. H.; ENORÉ, D. P.; BISCARO, T. S. Characteristics of a hailstorm that occurred in Santa Rita do Sapucaí-MG, Brazil, in October 2019. **Ciência e Natura, Santa Maria**, v. 44, e46, 2022. DOI: https://doi.org/10.5902/2179460X65529.